CORROSION SCIENCE AND TECHNOLOGY, Vol.16, No.4(2017), pp.209~225
[Review Paper]
pISSN: 1598-6462 / eISSN: 2288-6524
DOI: https://doi.org/10.14773/cst.2017.16.4.209

An Overview on Hydrogen Uptake, Diffusion and Transport Behavior of Ferritic Steel, and Its Susceptibility to Hydrogen Degradation

Sung Jin Kim[1] and Kyoo Young Kim[2,†]

[1]*Department of Advanced Materials Engineering, Sunchon National University Jungang-ro, Suncheon 57922, Republic of Korea*
[2]*GIFT, Pohang University of Science and Technology (POSTECH), Hyoja-Dong, Pohang 37673, Republic of Korea*

(Received June 13, 2017; Revised June 13, 2017; Accepted June 23, 2017)

Development of high strength steel requires proper understanding of hydrogen behavior since the higher the steel strength the greater the susceptibility of hydrogen assisted cracking. This paper provides a brief but broad overview on hydrogen entry and transport behavior of high-strength ferritic steels. First of all, hydrogen absorption, diffusion and trapping mechanism of the steels are briefly introduced. Secondly, several experimental methods for analyzing the physical/chemical nature of hydrogen uptake and transport in the steels are reviewed. Among the methods, electrochemical permeation technique utilized widely for evaluating the hydrogen diffusion and trapping behavior in metals and alloys is mainly discussed. Moreover, a modified permeation technique accommodating the externally applied load and its application to a variety of steels are intensively explored. Indeed, successful utilization of the modified permeation technique equipped with a constant load testing device leads to significant academic progress on the hydrogen assisted cracking (HAC) phenomenon of the steels. In order to show how the external and/or residual stress affects mechanical instability of steel due to hydrogen ingress, the relationship among the microstructure, hydrogen permeation, and HAC susceptibility is briefly introduced.

Keywords: *ferritic steel, hydrogen uptake, hydrogen permeation, hydrogen assisted cracking*

1. Introduction

The hydrogen is the smallest in atomic radius and the simplest in electronic structure among the elements on periodic table. Due to the intrinsic nature of the hydrogen atom, it can readily diffuse into the steel, which makes the steel susceptible to hydrogen embrittlement or hydrogen delayed fracture [1]. It is generally understood that the fine atomic hydrogen introduced in the steel matrix diffuses through the interstitial lattice sites of iron [2]. Particularly, at low temperature below 500 K, the hydrogen atom prefers to occupy tetrahedral sites in the body centered cubic (BCC) lattice, but, at high temperature, it can simultaneously occupy both tetrahedral and octahedral sites. Generally, tetrahedral interstitial sites are more favorable for the hydrogen atom since the sites have larger free volume size than the other sites [2,3]. Most commercial steel alloys, however, have a variety of metallurgical defects and imperfections in it, such as grain/phase boundary, dislocation, interface between the steel matrix and the 2nd phase particles etc. Since the energy level around the defects is higher than that in normal lattice sites, hydrogen atom can be preferentially trapped at the defects reversibly or irreversibly depending on the hydrogen binding energy and activation energy for hydrogen release. This trapping process leads markedly to reduce the mechanical properties such as ductility and impact toughness, frequently resulting in hydrogen assisted cracking (HAC) or delayed fracture [4,5]. In particular, the steels used for transportation and/or processing of oil and gas containing H_2S have been suffered from the HAC failure since the hydrogen is more easily introduced into the steels due to the poisoning effect by H_2S [6,7]. The poisoning effect caused by H_2S and adsorption of atomic hydrogen on the steel surface are discussed in more detail in the following section. Actually, the HAC failure of the steels can be classified into two different types depending on the presence of stress; one is hydrogen induced cracking (HIC) occurring under no applied stress [8,9] and the other is sulfide stress cracking (SSC) occurring under applied tensile stress or residual stress [10,11].

The other steel that is vulnerable to hydrogen degradation is advanced high–strength steels with tensile strengths more than 980 MPa such as transformation induced plasti-

†Corresponding author: kykim@postech.ac.kr

city (TRIP) steel, dual phase (DP) steel, complex phase (CP) steel and twinning induced plasticity (TWIP) steel. Recently, there has been increasing demands for development of advanced high–strength steels due mainly to their excellent mechanical properties. However, they are known to easily suffer a newly emerging problem of hydrogen delayed fracture (HDF) since the susceptibility to HDF increases proportionally with the level of their strength [12-15]. In such cases, the source of hydrogen is closely associated with the atomic hydrogen reduced from the neutral water on the steel surface [15,16]. Adsorption of atomic hydrogen on the steel surface exposed to the neutral environment is discussed in more detail in section 2.2.

A considerable body of literature has reviewed the hydrogen degradation phenomena occurring in various steel alloys, and a variety of hydrogen degradation models have been proposed by numerous researchers [17-21]. Moreover, in order to understand clearly hydrogen degradation phenomena, a lot of researchers have focused their attention on verifying the exact physical and chemical nature of hydrogen uptake and transport in the steels [22]. For this, various methods and instruments for the determination of the hydrogen diffusion behavior in steels have been proposed and developed. Firstly, two kinds of measurement of diffusible hydrogen content in steels using glycerin method and mercury method were developed, and they have been standardized in ISO 3690 [23] and JIS Z3113 [24], respectively. Secondly, the thermal desorption spectroscopy (TDS) using gas chromatograph known to be effective to measure the content of hydrogen trapped irreversibly as well as reversibly has been developed. Thirdly, the electrochemical permeation technique was developed in 1962 by Devanathan and Stachurski [25], and it has been standardized in ISO according to 17081 [26]. In particular, the permeation technique has been widely utilized for over fifty years since the technique imparts various hydrogen diffusion parameters within a few hours without any calibration operation. Since 1970s, the influence of externally applied tensile stress on hydrogen permeation through a variety of metallic materials has been extensively investigated [27-34]. For this, the permeation cell has been modified by equipping with a constant load testing instrument, so that the tested metallic material can be subjected simultaneously to the hydrogen charging and tensile straining during the permeation measurement. However, under the high level of tensile stress, the side effect caused by the pre–mature disruption of thin palladium (Pd) coating layer deposited on the detection side of the steel membrane has been reported [30,31,35]. The basic principle of the permeation technique and its inherent problem under the stress condition are introduced in section 4.

Since 1980s, the study on clarifying the relationship among the microstructure, hydrogen permeation, and HAC susceptibility of the steel has been progressed by means of the permeation technique [8,36-42]. Due to the development of advanced steel making process and thermal mechanical controlled process (TMCP), the microstructure has been optimized for higher resistance to the HAC failure. More detailed information is provided in the last section of this literature.

2. Hydrogen diffusion and trapping mechanism

2.1. Hydrogen adsorption/absorption mechanism in sour condition

The entry of hydrogen into the steel matrix is caused by the adsorption of hydrogen atom (H) which is cathodically reduced from hydrogen cation (H^+) dissociated from H_2S gas in aqueous medium [43]. It is generally known that, for the reduction of H^+, the following electrochemical reactions are involved [44].

$$\text{(Anodic reaction)}\quad Fe \rightarrow Fe^{2+} + 2e^- \qquad (1)$$

$$\text{(Cathodic reaction)}\quad H^+ + e^- \rightarrow H \qquad (2)$$

These reactions mean that the H^+ is reduced to the atomic hydrogen by accepting the electron generated by the anodic dissolution of iron. Since atomic hydrogen is thermodynamically unstable, it tries to be hydrogen molecule quickly by the recombination reaction ($H + H \rightarrow H_2$). However, H_2S gas dissolved in the aqueous environment inhibits effectively the recombination reaction and consequently, a large amount of hydrogens in an atomic form are readily adsorbed on the steel surface and introduced into the steel matrix [8]. The hydrogen entry mechanism described here has also been illustrated in the previous study [43]. Actually, the significant increase in hydrogen content in the steels exposed in sour environment has been experimentally demonstrated by numerous researchers [8,45,46]. Moreover, there have been lots of mechanistic studies of the enhancement of hydrogen adsorption on the steel surface and diffusion into the steel matrix because of the poisoning effect by H_2S [6,7,47,48]. Firstly, in 1965, Bockris *et al.* [47] and Bolmer [48] have proposed the mechanistic models for hydrogen diffusion. However, the models have been considered to be incomplete system since it is difficult to obtain the reaction parameters for the hydrogen evolution and hydrogen adsorption. Then, in 1974, Iofa *et al.* [6] have developed the poisoning mechanism. According to their study, HS^- anion dis-

sociated from H_2S accelerates the discharge of H^+ ion. However, their model and its interpretation have also been considered as incomplete system due to unknown reaction parameters like the case of the other models. Furthermore, in general acid environment, there would be much higher concentration of H_2S compared to HS^- owing to much lower solubility of H_2S. In 1976, Kawashima *et al.* [7] have presented the following reaction model which can be applied particularly in acid environment.

$$\text{Step 1: } H_2S_{ads} + e^- \rightarrow H_2S_{ads}^- \quad (3)$$
$$\text{Step 2: } H^+ \rightarrow H_{ads}^+ \quad (4)$$
$$\text{Step 3: } H_2S_{ads}^- + H_{ads}^+ \rightarrow H_2S{\sim}H_{ads} \text{ (unstable)} \quad (5)$$
$$\text{Step 4: } H_2S{\sim}H_{ads} \rightarrow H_2S_{ads} + H_{ads} \quad (6)$$

According to this model, it is assumed that the electrical attraction between $H_2S_{ads}^-$ and H_{ads}^+ formed by the step 1 and 2, respectively, produces a complex compound of $H_2S{\sim}H_{ads}$, identified in step 3. Since it is known that the compound tends to be unstable, it is readily dissociated and consequently, atomic hydrogen can be adsorbed on the steel surface and introduced in the steel matrix.

2.2. Hydrogen adsorption mechanism in ambient atmosphere

Advanced high–strength steels for bolt or automotive body are commonly used in ambient atmosphere. In such cases, the main source of hydrogen can be assumed to be the atomic hydrogen which is cathodically reduced from the neutral water condensed normally on the steel surface [15,16]. In general, the pH in the water layer on the steel surface would be neutral in atmospheric environments and therefore cathodic reaction is supposed to be oxygen reduction ($O_2 + 2H_2O + 4e^- \rightarrow 4OH^-$). This means that the hydrogen evolution reaction hardly occurs, and a decrease in pH and low corrosion potential are required for the hydrogen evolution reaction. Tsuru *et al.* [15] have reported that when the pre-formed rust layer on the steel surface is moistened, corrosion and hydrolysis reactions lead to decrease the pH level and corrosion potential where the hydrogen evolution reaction proceeds. The corrosion and hydrolysis reactions proposed are as follows:

$$Fe \rightarrow Fe^{2+} + 2e^- \quad (7)$$
$$Fe^{2+} + 2H_2O \rightarrow Fe(OH)_2 + 2H^+ \quad (8)$$

The enhancement of hydrogen entry with progress of corrosion and the growth of rust layer has also been observed by Akiyama *et al.* [12] According to them, hydrogen entry into AISI 4135 steel increases with increase in cyclic corrosion test number and humidity level. Furthermore, the mechanism of hydrogen entry into high–strength steel with tensile strength more than 1225 MPa suffering from the delayed fracture has been suggested by Omura *et al.* [16] The hydrogen entry mechanism proposed by Omura *et al.* [16] can be explained by the following a series of reactions:

1) Anodic dissolution of the steel and Fe^{2+} ion is generated
2) Oxidization of Fe^{2+} into Fe^{3+} ions
3) Hydrolysis of Fe^{3+} accelerated by Cl^- ions, followed by a pH drop
4) Hydrogen evolution, resulting in hydrogen entry

They have also investigated the environmental factors affecting hydrogen entry into the steel by the permeation experiment under wet-dry cyclic conditions. They have indicated that temperature, relative humidity, and the amount of sea salt considered to be Cl^- ion concentration on the steel surface can affect strongly the hydrogen introduction into the steel. Particularly, hydrogen permeation coefficients are higher at 40 ~ 60% of relative humidity level since Cl^- ion concentrates in the water layer at the particular humidity level, leading to the accelerated hydrolysis of Fe^{3+}, resulting in a pH drop. The enhancement of hydrogen entry into a variety of high-strength steels has been considered to mainly/partly be responsible for the delayed fracture.

2.3. Hydrogen diffusion and trapping theory

As for the interactions between hydrogen atom and a variety of trap sites in steel, hydrogen atom can easily interact with various defects in crystals. Particularly, at short ranges, the hydrogen atoms interact chemically through localized bonding [49]. Metallurgical defects and

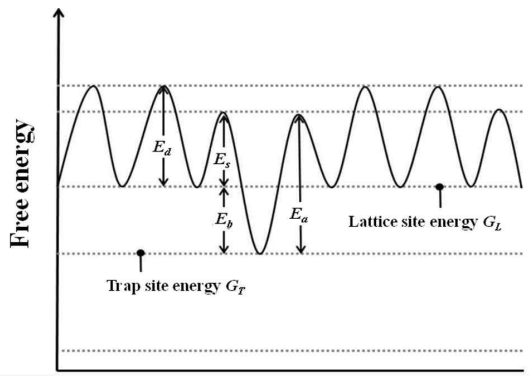

Fig. 1 Energy level of hydrogen around trap sites: E_d, diffusion activation energy in normal lattice; E_s, saddle point energy; E_a, trap activation energy. The binding energy is a difference between the lattice site energy G_L and trap site energy G_T ($E_b = G_L - G_T$) [55].

imperfections such as vacancies, dislocation, grain/phase boundary, interfacial gap between the steel matrix and the precipitate/inclusion etc., can act as trapping sites for hydrogen atoms [22,50-52]. In general, the hydrogen introduced in the steel is classified into three types of category; interstitial-lattice diffusing hydrogen, reversibly trapped hydrogen and irreversibly trapped hydrogen. The hydrogen traps are generally divided into two categories; reversible and irreversible traps according to the hydrogen binding energy and the activation energy for hydrogen release [26,52-54]. The free energy of the hydrogen-steel system can be briefly described as Fig. 1 [55]. Since the free energy of hydrogen atoms residing at trap sites is lower than that at lattice sites, they prefer to occupy the trap sites. The trap sites are considered irreversible if the trapped hydrogen is not released at room or at low temperatures. On the other hand, hydrogen at reversible traps can be readily trapped and released from the sites even at low temperature, and they play a combined role of sink and/or source for hydrogen atoms because they can absorb and release the hydrogen atoms [53,54,46]. This means that hydrogen atoms can migrate easily through a crystal lattice, and they can weaken the cohesive strength between Fe-Fe atoms, and cause additional stress due to the local lattice distortion. Consequently, the steel can be embrittled and the tensile ductility and impact toughness can be significantly reduced, often resulting in HAC failure. This mechanism is generally known as decohesion theory proposed by Troiano [17]. Some researchers have indicated that those traps with binding energy less than 60 kJ/mol are termed reversible traps, while those with higher than 60 kJ/mol are called irreversible traps [57]. Among various trapping sites in steel alloys, the binding energy for hydrogen release from grain boundary

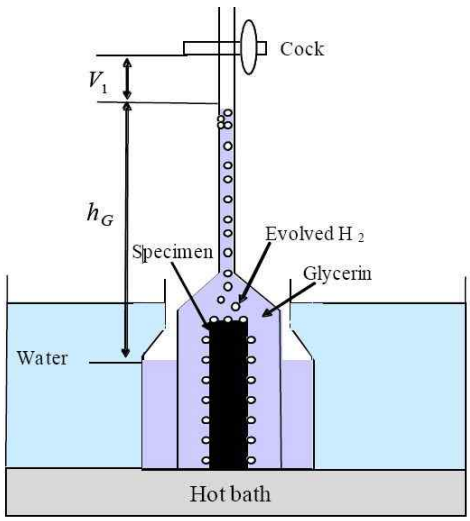

Fig. 2 A schematic illustration of the glycerin method [45].

and dislocation are reported to be 18.2 kJ/mol and 26.8 kJ/mol, respectively, which are significantly lower value than those of 2nd phase particles (non–metallic inclusions or precipitates) such as MnS (72 kJ/mol), Al_2O_3 (86.2 kJ/mol) and TiC (94.6 kJ/mol) [22,57-59]. Therefore, the grain boundary and dislocation are classified as the reversible trapping site, and MnS, Al_2O_3 and TiC are classified as the irreversible trapping sites for hydrogen atoms. In the case of retained austenite and the interfacial gap between the steel matrix/Fe_3C, there is some controversy [22,60-65]. Values of the binding energies for a number of hydrogen traps in ferrous alloys are listed in Table 1 in the order of increasing trap-hydrogen binding energies. In general, both lattice diffusing hydrogen and reversibly trapped hydrogen are referred to the diffusible hydrogen

Table 1 Hydrogen binding energy of various trap sites in α–iron

Trap site	Binding activation energy (kJ/mol)	Ref.
Interstitial solutes	3~15	22
Grain boundary	9.6	22
Dislocation elastic stress field	20	66
Dislocation core	59	51
AlN-Ferrite matrix interface	65	67
Free surface	70-95	69
MnS-Ferrite matrix interface	72	70
Al_2O_3-Ferrite matrix interface	79	55
Fe_3C-Ferrite matrix interface	84	68
TiC-Ferrite matrix interface	87	71

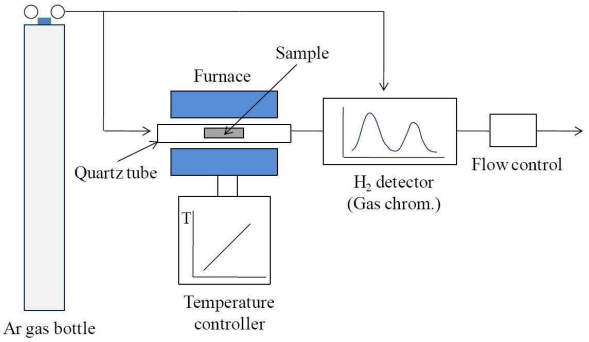

Fig. 3 Typical set-up for thermal desorption spectroscopy (TDS) [52].

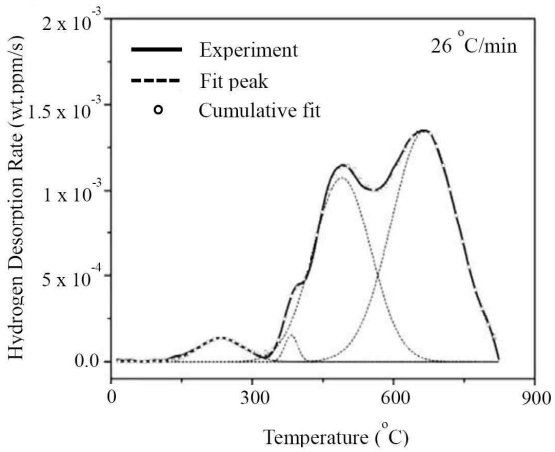

Fig. 4 TDS test result appeared in Fe-Mn-Al-C containing austenitic steel shows four hydrogen desorption peaks [76].

which is known to be mainly responsible for the embrittlement of the steel.

3. Hydrogen measurement method

3.1. Glycerin and mercury method

The glycerin method was firstly introduced in the AWS specification A5.5–48T (ASTM A316–48T) in 1948 [72]. A simple schematic of the glycerin method is depicted in Fig. 2. The experimental procedure can be summarized as follows [45]:

Step 1: Hydrogen charging into the specimen

Step 2: Right after the charging, specimen is inserted into glycerin. During this process, liquid nitrogen or ice water can be used as a medium to prevent hydrogen diffuse out from the specimen.

Step 3: After collecting diffusible hydrogen content from the specimen for two days, the diffusible hydrogen content can be measured by the following equation:

$$V(ml) = \frac{(h_{l,G} - h_G)V_1 273.15}{8.2(273.15 + T_1(^oC))}$$

where V_1 specifies the hydrogen content released from a specimen, *8.2* refers the height of glycerin column at standard temperature and pressure, $h_{l,G}$ is the height of glycerin column at 0 °C and atmospheric pressure, h_G is the height of glycerin column at T_1 and atmospheric pressure where T_1 is measured temperature.

Shortly after its introduction, Stern *et al.* [73] suspected the suitability of glycerin as a hydrogen collection medium due mainly to partial dissolution of hydrogen in glycerin as well as poor reproducibility. For this reason, mercury has become the alternative as a hydrogen collection medium since the solubility of hydrogen in mercury is extremely low level [74,75]. However, mercury method has not been widely utilized since it is known as one of the environmental hazard and toxic materials. Furthermore, main limitation for the two methods is that the diffusible hydrogen content in the steel can only be obtained. No other information about diffusion parameters for hydrogen atom can be provided. Nevertheless, the glycerin method has been frequently employed to measure the diffusible hydrogen contents in ferritic steels.

3.2. Thermal desorption spectroscopy (TDS)

The thermal desorption spectroscopy using gas chromatograph is effective to measure the content of hydrogen trapped both reversibly and irreversibly by heating the steel sample at high temperature above 800 °C. The typical set-up for TDS is illustrated in Fig. 3 [52]. Basically, the charged sample with hydrogen is heated in a chamber flushed continuously with argon gas, and the evolved hydrogen gas can normally be detected by a thermal conductivity detector. Under a constant heating rate, hydrogen desorption peaks from different types of traps can be obtained. The test results for austenitic steel with Fe-Mn-Al-C are simply described in Fig. 4 [76]. As exhibited, several types of trap in the steel sample result in four distinctive peaks in the hydrogen desorption curve. According to the authors, the first peak is mainly attributed to the hydrogen trapped at low energy barrier sites such as grain boundary and the elastic field of an edge dislocation. Peaks 2 and 4 are closely associated with hydrogen desorption from precipitates with high activation energies. However, as for desorption peak 3, the trapping nature could not be decided precisely.

In addition, the activation energy of various trapping sites in the steel can be calculated using the equation pro-

posed by Kissinger *et al.* [77]. A generic model proposed by Kissinger is similar to chemical reaction rate theory [78]. Under certain condition, the theory can be applied to hydrogen desorption process developed by Choo *et al.* [22], and the activation energy for hydrogen release, E_T, can be calculated as follows:

$$\frac{dx}{dt} = A(1-x)exp\{\frac{-E_T}{RT}\} \qquad x = \frac{H_0 - H_t}{H_0}$$

where H_0 and H_t refer the original and instantaneous hydrogen concentrations in the steel, x is the fraction of hydrogen released, A is the rate release constant, R is the gas constant, T is the absolute temperature, and t is the time.

Under a constant heating rate ($\lambda = dT / dt$), the maximum rate for hydrogen release from a trap can be achieved by differentiating the above equation, and taking the log of both sides, and consequently the following Kissinger equation can be derived [52,77,79].

$$\frac{\partial \ln(\lambda / T_c^2)}{\partial(1/T_c)} = -\frac{E_T}{R}$$

where T_c specifies the temperature at which maximum hydrogen desorption rate.

The TDS using gas chromatography is especially useful tool to measure the hydrogen content absorbed in the irreversible trap sites such as MnS, TiC and Al_2O_3. By using the TDS, valuable information about the hydrogen trapping phenomenon in a variety of steels has been reported in a number of literature [64,80-82]. However, there are several inherent difficulties in utilizing the TDS for evaluation of the body centered cubic (BCC)-based materials. Due to the high diffusivity of hydrogen (~10^{-9} m^2/s) [2] in the BCC structure, it is possible for the lattice and reversibly trapped hydrogen to diffuse rapidly out of the ferritic steels before the onset of measurement by the TDS. For this reason, the TDS has been widely employed in hydrogen analysis of the steels containing FCC structure with much slower hydrogen diffusivity (~10^{-16} m^2/s) [83]. Another limitation of TDS method is based on the assumption that the hydrogen evolution from the steel sample is the same as the hydrogen released from trap sites, meaning that the interstitial lattice diffusion of hydrogen can be neglected. This assumption is valid when there is no hydrogen accumulation in the sample. At high heating rate, it is difficult for hydrogen degassing through lattice diffusion to keep up with the change in temperature, leading to hydrogen accumulation in the sample. On the contrary, at low heating rates, there is local equilibrium between lattice and trap site, which allows hydrogen capture by the traps and hydrogen release from the traps [50]. Considering these facts discussed above, TDS has both advantages and limitations for the analysis of hydrogen in steel alloys. Utilization of TDS instrument in actual industrial sectors have contributed much to the development of high performance steel plate and its welding material exhibiting superior resistance to HAC and HDF.

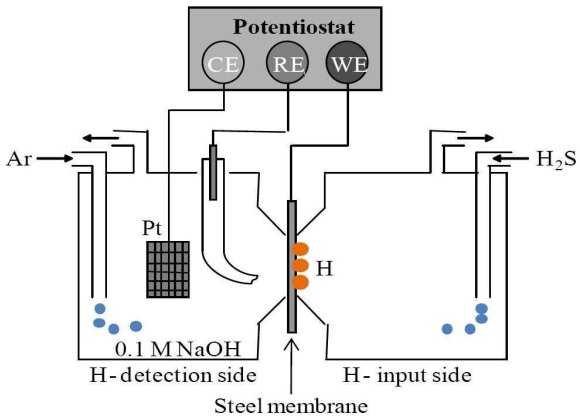

Fig. 5 A simple schematic diagram of the electrochemical permeation technique [45].

3.3. Electrochemical hydrogen permeation technique

The electrochemical permeation experiment was firstly developed in 1962 by Devanathan and Stachurski [25] and it has been standardized in ISO according to 17081 [26]. The permeation technique involves the introduction of atomic hydrogen generated on one side (hydrogen charging side) of a steel membrane in aqueous medium under cathodic polarization condition, the diffusion process through the thin membrane, and the releasing process from the membrane on the other side (hydrogen detection side). Basically, the permeation flux can be evaluated by measuring the hydrogen oxidation current density on the detection side of the membrane electroplated with thin film of Pd or Ni to which a constant anodic potential is applied. Fig. 5 presents a simple schematic diagram of the electrochemical permeation technique. Utilization of this technique makes it possible to determine various diffusion parameters for hydrogen atoms such as apparent hydrogen diffusivity, solubility, and permeability. Although an alternative permeation technique employing the gas phase charging method has been proposed [84], and it has proved that the method can provide easy control of inlet hydrogen fugacity, but it was found impractical at low

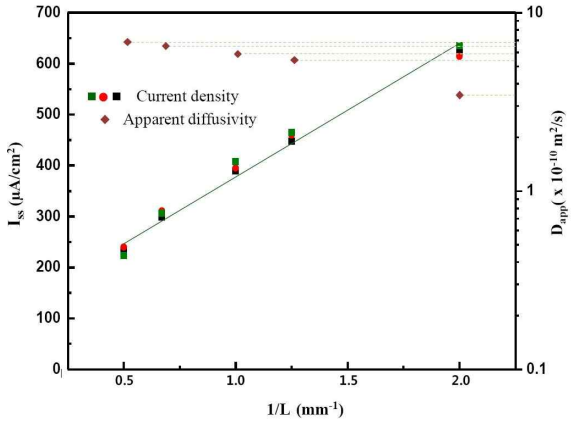

Fig. 6 Steady-state permeation current density and apparent hydrogen diffusivity (D_{app}) with reciprocal thickness (L) under cathodic charging of 2 mA/cm^2 [92].

temperature measurement due mainly to the surface impedance problem [52,84,85]. This problem limits application of the gas phase charging method to the permeation experiment conducted especially at low temperature [83]. One of the important features of the permeation technique is that thin steel membrane located in the center of the permeation test cell should be controlled by the volume diffusion [86]. The volume controlled diffusion is achieved when hydrogen diffusion through the steel membrane is slower than the kinetics of surface reaction related with hydrogen reduction. When the membrane thickness exceeds the critical value, it can follow the Fick's law of diffusion, exhibiting the relationship between the permeation current density (i_{ss}) at steady-state and membrane thickness, which is as follows [84]:

$$i_{ss} = \frac{D_{app} C_0}{L}$$

where D_{app} is the apparent hydrogen diffusivity, and C_0 is the sub-surface hydrogen concentration on hydrogen charging side.

According to the experimental results presented by Kitel *et al.* [86], for the ferritic carbon steel immersed in electrolyte under no applied potential, the critical thickness ensuring the volume controlled hydrogen transport through the steel is around 2 mm. However, other researchers [8,32,87-91] have conducted the permeation test using the thinner steel membrane with 1 mm thickness or below under cathodic polarization, and they have provided conflicting results. Although the verification of membrane thickness controlled purely by volume–diffusion is of great importance in the academic circles, the controversy over the volume diffusion condition has been around for many years, and this makes researchers to question the reliability and accuracy of measured permeation data. Recent study conducted by Kim *et al.* [92] has revealed that the permeation flux evaluated under cathodic polarization of 2 mA/cm^2 is inversely proportional to the steel thickness even 0.5 mm, which meets well with Fick's law of diffusion. Based on their study, it is expected that, under cathodic polarization on the steel in the deaerated acidic solution, the surface reaction kinetics can be faster than the volume diffusion, and therefore the diffusion through the steel membrane can be the rate determining step [92]. Fig. 6 exhibits the relationship between the steady-state permeation current density and reciprocal thickness ranging from 0.5 mm to 2 mm, presented by Kim *et al.* [92]. A recent study conducted by Ha *et al.* [81] has also reported that the thinner membrane just over 448 μm thickness under cathodic polarization condition can be controlled by volume diffusion. For clarification on the experimental demonstrations, further academic discussion would be required.

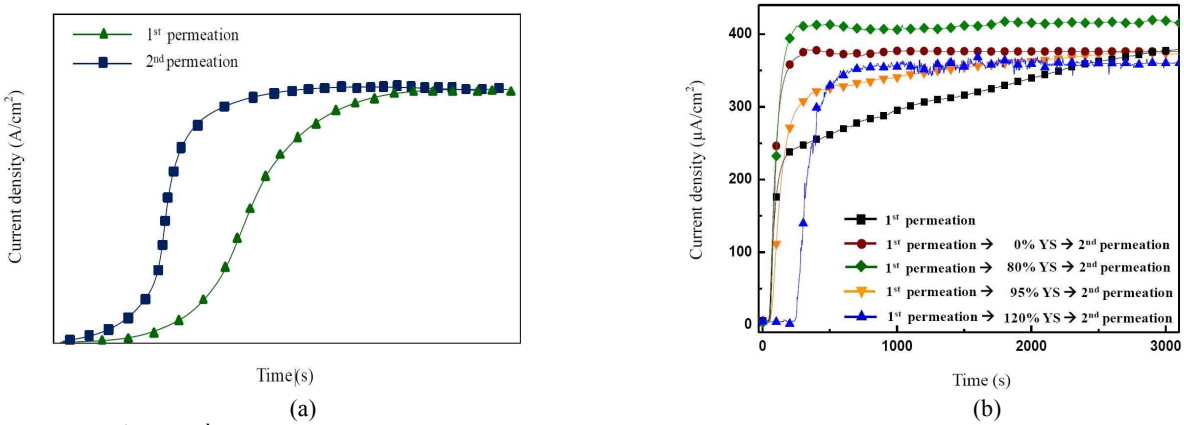

Fig. 7 Typical 1st and 2nd permeation transients [95].

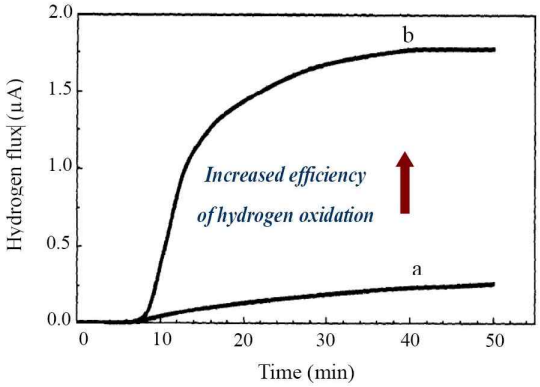

Fig. 8 Measured hydrogen oxidation rate with and without the Pd coating on hydrogen detection side in the permeation test [96].

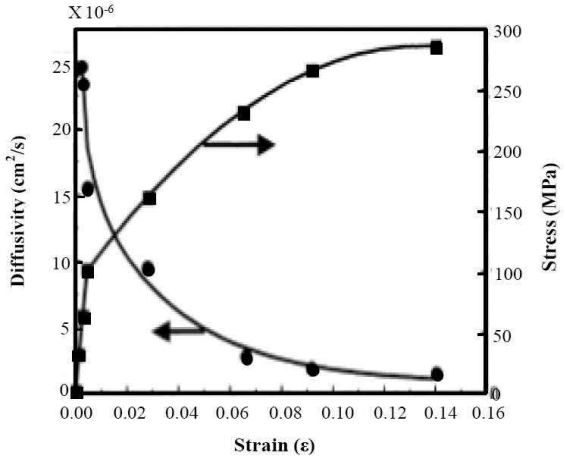

Fig. 9 Change in apparent hydrogen diffusivity (D_{app}) in iron with static tensile stress conditions [4].

One of the advantages of electrochemical permeation technique is that, from the two consecutive permeation (1st and 2nd permeation) transients, it is possible to estimate an order of magnitude of irreversible trapping without the use of TDS analysis since the area between 1st and 2nd permeation curves provides an approximation of irreversible trapped hydrogen contents [93-95]. Fig. 7 exhibits typical 1st and 2nd permeation behaviors [95]. As noticed in Fig. 7, 1st permeation shows longer breakthrough time. Since all of the irreversible traps are occupied by hydrogen atoms during the 1st permeation, hydrogen atoms contained only in the interstitial-lattice and reversible traps are considered in the 2nd permeation. Consequently, 2nd or 3rd permeation exhibits faster diffusion kinetics and the time to reach the steady state flux becomes shorter [94]. Fig. 7b exhibits the overlapped view of 1st and 2nd permeation behaviors of ferritic steel under various tensile stress conditions. It is found that the time to reach the steady-state current density is much shorter in 2nd permeation transient under no applied load. However, the breakthrough time increases slightly with increasing the applied load, which is closely associated with the formation of local-plastic region under high level of tensile stress in elastic regime. Upon exceeding the elastic limit, the permeation curve shows much longer breakthrough time because of newly generated dislocation during the plastic deformation of the steel.

The electrochemical permeation method has been modified to accommodate the externally applied tensile load because the effect of applied stress on hydrogen diffusion through the steel has been one of the most important aspects of the hydrogen assisted cracking failure [4,30-32]. Actually, this permeation method has been successfully employed by plating palladium (Pd) on the hydrogen detection side of the steel membrane. Since the thin layer of Pd coating acts as a catalyst for hydrogen oxidation ($H \rightarrow H^+ + e^-$), the fact whether the Pd is uniformly coated on the steel surface or not can be one of the crucial factors for the permeation experiment. Fig. 8 illustrates the effect of Pd on the efficiency of hydrogen oxidation reaction on the hydrogen detection side in the permeation test [96]. Considering this fact, the failure (plastic deformation) of Pd coating layer during the permeation experiment for high strength steels under loading conditions can be a critical problem, and the obtained permeation data cannot be reliable [35]. This problem and some proposed solutions are discussed in more detail in later section.

4. Effect of tensile stress on hydrogen permeation

4.1. Hydrogen permeation test under applied loads

Since 1970s, the effect of externally applied stress on hydrogen permeation through various metallic materials has been extensively investigated by numerous researchers [4,30,31-33,97]. For this, the permeation experiment has been carried out with a modified Devanathan and Stachurski cell equipped with a constant load testing apparatus, so that the tested specimen can be subjected simultaneously to the hydrogen charging and tensile straining during the permeation measurement. By using the modified permeation technique, lots of valuable information about the influence of applied tensile load on hydrogen diffusion behavior in both elastic and plastic regime of a variety of metallic materials has been provided. Since Bastien *et al*. [98] proposed that dislocations formed under plastic deformation could carry hydrogen atom in the form of Cottrell atmospheres, the relationship between plastic de-

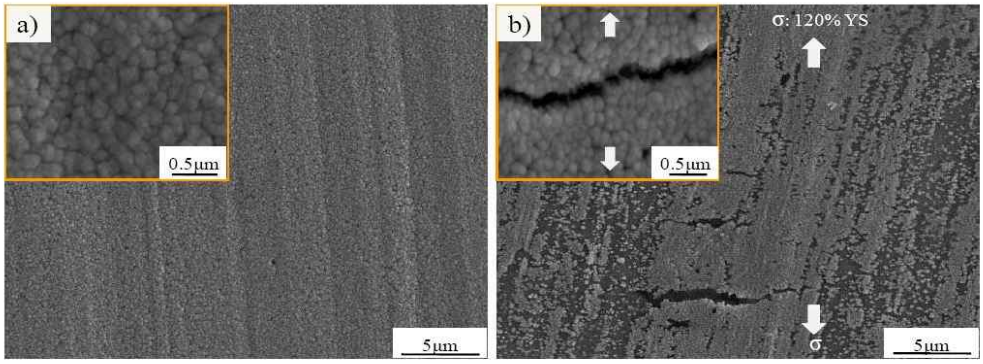

Fig. 10 FE-SEM photographs showing the morphology of Pd coating layer formed on (a) steel surface before applying the tensile stress; (b) steel surface after applying the tensile stress corresponding to 120% YS of steel substrate [35].

formation and hydrogen diffusion behavior in metallic materials has been extensively studied. Kurkela *et al*. [27] have also supported the idea that mobile dislocations can carry hydrogen atoms and the experimental evidence that the apparent hydrogen diffusivity in Ni increased by up to 5 orders of magnitude has been provided. Otsuka *et al*. [28] and Frankel *et al*. [99] have also observed the similar behavior for Ni. On the contrary, the permeation tests performed by Kurkela *et al*. [32] with a fully bainitic 2.25Cr–1Mo steel, and by Zakroczymski *et al*. [100] with pure iron have suggested that dislocation can act as trap for hydrogen atom and thus a sudden and substantial decrease in permeation flux at the onset of plastic deformation has been clearly identified. In addition, Huang *et al*. [4] have indicated that the hydrogen diffusivity decreases as the plastic deformation increases in the constant loading experiments with pure iron, indicating that hydrogen atoms are trapped at dislocations in the steel membrane. Consequently, it takes longer time for hydrogen to escape from the steel. This behavior is shown in Fig. 9. Kurkela *et al*. [32] have reported that the contradictory results between the studies with Ni and studies with ferritic steel alloy are mainly attributed to the difference in the binding energy between hydrogen and dislocation in the metallic materials. Based on their study, it can be assumed that the binding energy of hydrogen atom to dislocations in BCC-based alloys is much higher than that in FCC-based alloys. For this reason, the dislocations in BCC-based alloys generated by plastic deformation enhance the hydrogen trapping rather than transport, which contributes to the reduction in the apparent hydrogen diffusivity. On the other hand, Huang *et al*. [4] and Zheng *et al*. [101] have specified that, when a metallic material is plastically deformed, both the enhanced trapping and enhanced transport by dislocation can play a role, regardless of its crystal structure. Contrary to the plastic stress condition, the elastic stress is not considered to increase the concentration of hydrogen trap, and it is known that the elastic stress has no significant effect on the hydrogen diffusivity but has increased slightly the permeation flux owing to the interstitial lattice expansion [4,33,100]. Although Townsend *et al*. [102] have suggested that the increase in the permeation rate under the tensile stress in elastic range is closely associated with the increase in the exchange current density for the hydrogen reduction reaction on the steel surface under the stress regime, it has not been experimentally proved. On the other hand, Kim *et al*. [5] has proposed an alternative explanation about the increase in permeation flux of the ferritic steel under applied tensile stress in elastic range. They have indicated that the corrosion product of FeS_x formed naturally on the steel in sour environment acts as sites for hydrogen reduction reaction, and the applied elastic stress weakens the stability of the product by forming lots of cracks in the local sulfur deficient region. However, there still remain uncertainties about the phenomenon.

In spite of lots of efforts to clarify the effect of tensile stress on hydrogen uptake and transport behavior of a variety of metallic materials employing the permeation technique, it has been limited to low-strength steels with yield strength lower than that of Pd, due to pre–mature failure of Pd layer deposited to the detection side of the membr ane under high level of applied tensile stress [31,35]. The application of high level of tensile stress exceeding the elastic limit of the Pd (< 205 MPa) lead essentially to the plastic deformation of Pd coating layer. As a result, little academic progress on SSC phenomenon occurring under stress condition has been made. For this reason, Kim *et al*. [35] has proposed a simple permeation technique applicable under tensile stress even in plastic range.

The unstable background current density and unreliable permeation current density caused by the pre-mature rupture of thin Pd coating layer under applied stress over YS of Pd layer are discussed in more detail in the following section.

4.2. Inherent problem in the permeation test under loading condition and its solution

As described earlier, for a steel membrane under externally applied tensile stress, the reliability of the permeation experiment depends greatly upon the stability and integrity of the thin Pd film. When a Pd-coated steel membrane is subjected to either higher applied stress than the YS of the steel or much higher percentage elongation than the total elongation of bulk Pd, the thin layer of Pd can be plastically deformed and ruptured. Kim *et al*. [35] have clearly demonstrated that a significant change in background current in the form of a current spike appears whenever the constant load above the YS of Pd is applied. The experimental results exhibiting the change in background current density with constant tensile stress up to 120% YS of the steel substrate can be found in their study, and disrupted Pd layer under the stress condition are presented in Fig. 10 [35].

In order to avoid the problem with the disruption of the Pd film deposited on to high-strength Cr-Mo steels with YS of around 580-660 MPa during straining, Brass and Chêne [30] have performed the permeation experiment without Pd coating, and much lower current density has been obtained due to the absence of Pd layer acting as an effective catalyst for hydrogen oxidation. On the other hand, Park *et al*. [31] have devised a method. They have used an iron oxide film formed anodically in 0.1 M NaOH solution to replace the Pd deposition in the permeation test, providing consistent and reproducible permeation data. Nevertheless, the hydrogen oxidation current is still much low level comparing to the current level obtained employing a Pd film. For this reason, Kim *et al*. [35] have tried to solve this inherent problem of pre-mature deformation of coating layer under the loading condition. According to their study, instead of the Pd coating before tensile loading, the loading process was performed prior to the coating process. Although it appears that the concept of devised method is very simple, close attention is required in actual implementation of the method. Based on the modified sequence of the permeation test, the deformation problem of the Pd film can be fully eliminated, ensuring the stable background current density even under high level of tensile stress above YS of Pd. This has been experimentally evidenced by the previous work [35]. Moreover, they have proposed a stepwise

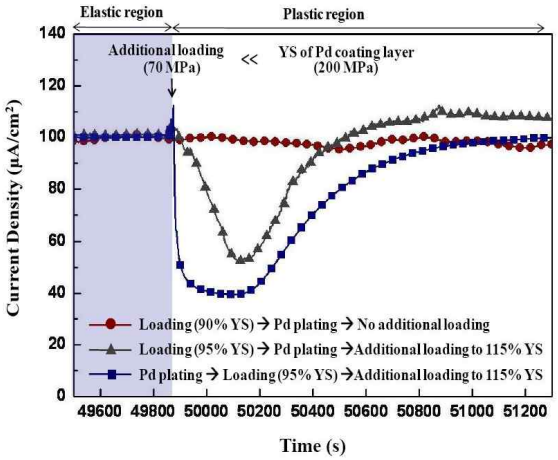

Fig. 11 The changes in hydrogen permeation current in the transient range from elastic to plastic stress [5].

sequence method to evaluate the effect of tensile stress on hydrogen diffusion behavior of various metallic materials in the permeation test. The modified permeation technique consists of: a stepwise sequence of elastic mechanical loading below YS of metallic materials, Pd plating followed by additional mechanical loading to plastic deformation. The utilization of this stepwise permeation sequence makes it possible to evaluate systematically the hydrogen permeation behavior in the transient range from elastic to plastic tensile stress of metallic materials by entirely excluding other side effects. One of the illustrations of the permeation behavior of ferritic steel in the transient state from elastic to plastic tensile stress, suggested by Kim *et al*. [5], is shown in Fig. 11. It is found from the Fig. 11 that after the initial drop of the permeation current upon application of plastic tensile stress, the current increases with time. The initial drop of the current is caused by the reversible trapping phenomenon of hydrogen atoms at newly generated dislocation in the steel subjected to plastic deformation. After initial drop of the current by enhanced hydrogen trapping, the enhanced hydrogen transport can also be predominant, leading to increase the overall permeation current. It is noticeable that the restored permeation current expressed as grey line is higher than that expressed as blue line. This difference in the hydrogen permeation current is attributed mainly to the decrease in hydrogen oxidation by the plastic deformation and disruption of the Pd film when tested by the conventional method (Pd plating → Loading (95% YS) → Additional loading to 115% YS) [5]. This stepwise permeation sequence can be considered to be a breakthrough to study more in depth the behavior of hydrogen in a wide range of high-strength steels under various mechanical

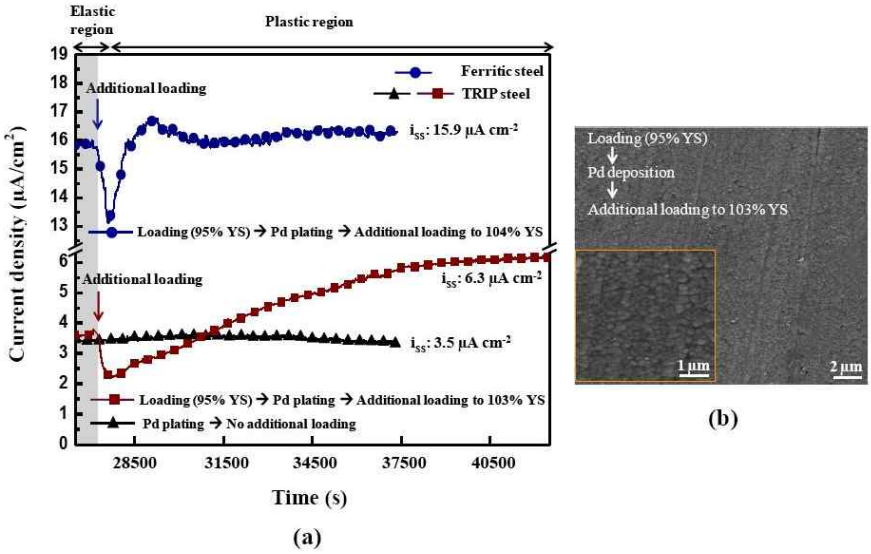

Fig. 12 (a) The changes in hydrogen permeation current in the transient range from elastic to plastic stress for two tested steels, ferritic steel and TRIP steel, and (b) The morphology of the Pd film layer obtained after the permeation test with stepwise sequence of 'elastic loading-Pd plating-additional loading to plastic range' [103].

loading conditions. This technique can be applied not only in the BCC-based steels, but also in the advanced high-strength steel containing some FCC-based phases in the microstructure. In particular, the change in hydrogen permeation flux under tensile stress condition of the phase transformation from γ to α' in the TRIP steel has been successfully evaluated. Fig. 12 shows that after an initial drop of the permeation current at the onset of plastic stress, the current level increases gradually, and continuously going up much higher comparing to the level of steady-state current [103]. This indicates that the hydrogen atoms in the TRIP steel are dictated by two kinds of transport process; one is predominant trapping by newly generated dislocation and the other is the change in diffusion kinetics by the phase transformation from γ to α' in the microstructure during the plastic deformation.

5. Effect of microstructure on hydrogen permeation and HAC failure

A considerable body of literature has concerned the relationship among the microstructure, hydrogen permeation behavior and HAC failure of the steel [8,36-42]. In 1980s, the effect of hydrogen on the mechanical properties of spheroidized carbon steels was studied utilizing the electrochemical permeation technique [36]. Particularly, Xie *et al*. [36] has focused their attention on the effect of cold work on hydrogen permeation and irreversible damage of spheroidized AISI 1090 steel. They have specified that application of cold work on the steel increases the steady state value of hydrogen fugacity at a given charging current and thereby lowers the critical value for hydrogen damage. In 1987, Johnson *et al*. [37,38] has investigated the correlation of microstructural parameters and hydrogen permeation behavior in carbon steel. According to their study, fine iron carbide and high carbon content correlate with a relatively high corrosion rate and lower permeability. Especially, iron carbides in pearlitic and quenched and tempered microstructures are predominately reversible traps for hydrogen atoms. In 1990s, Jeng *et al*. [39] has investigated the effect of pearlite morphology on hydrogen diffusion and solubility in carbon steel. In their study, hydrogen permeation behavior was evaluated with respect to the microstructures, spheroidized carbides in ferrite, tempered martensite and ferrite/pearlite mixture. They have revealed that the apparent hydrogen solubility (C_{app}) was lowest for spheroidized microstructure, intermediate for pearlitic microstructure, and highest for the quenched and tempered microstructures. The reason for the differences appears to be related with the magnitude of apparent hydrogen diffusivity (D_{app}) in each case. Since the carbide acts as obstacle to the transport of hydrogen and reversible trap for hydrogen, the spheroidized microstructure with lowest interfacial area between ferrite/carbide leads to the highest value of D_{app}, resulting in the lowest value of C_{app}. As for the permeation result of the steel having quenched and tempered microstructure, there has been controversy as to whether the microstructure ex-

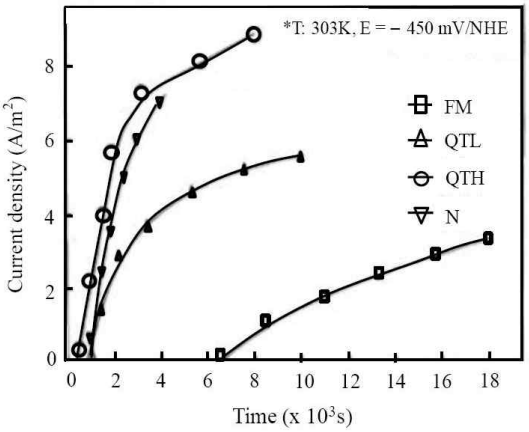

Fig. 13 Typical permeation transients of steel developed by various heat treatments (N: Normalized, FM: Fresh martensite, QTL: Quenched and tempered at low temperature, QTH: Quenched and tempered at high temperature) [40].

hibits the highest C_{app}. From recent studies, it has been demonstrated that the quenched and tempered microstructure is one of the most desirable microstructure for the high-strength steel having both high toughness and high resistance to HAC [8,46]. In the case of the untempered martensite, hydrogen trapping at a number of lath boundaries and dislocation arrays with high residual stress appears to be dominant, resulting in the lowest D_{app} and the highest C_{app}, which is generally accepted experimental phenomenon. The study conducted by Jeng *et al*. [39] has been consistent with the contention that the pearlitic steels are more susceptible to hydrogen embrittlement than spheroidized steels. In 1990s, Luppo *et al*. [40] and Luu *et al*. [41] have investigated that the influence of microstructure on hydrogen diffusion and trapping in carbon steels. In their study, a number of microstructures; typical ferrite/pearlite, fresh martensite and tempered martensite are

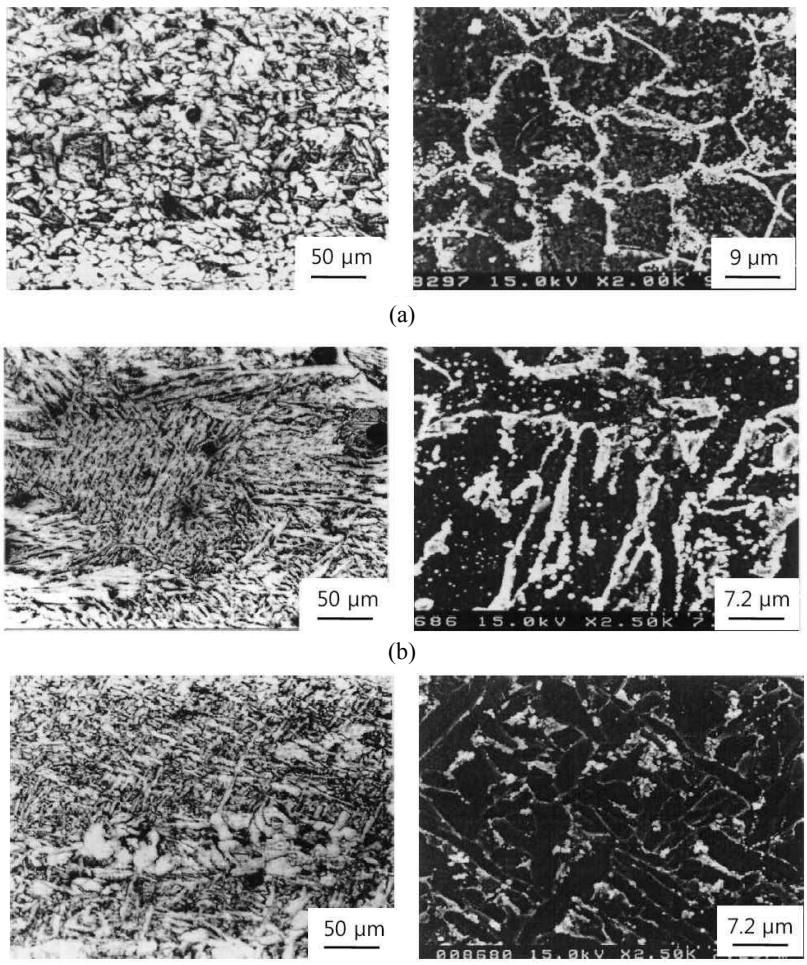

Fig. 14 Distribution of white silver grain at (a) ferrite grain boundaries and carbide/ferrite interfaces of finely scattered pearlite, (b) bainitic–lath interfaces and (c) acicular ferrite boundaries [88].

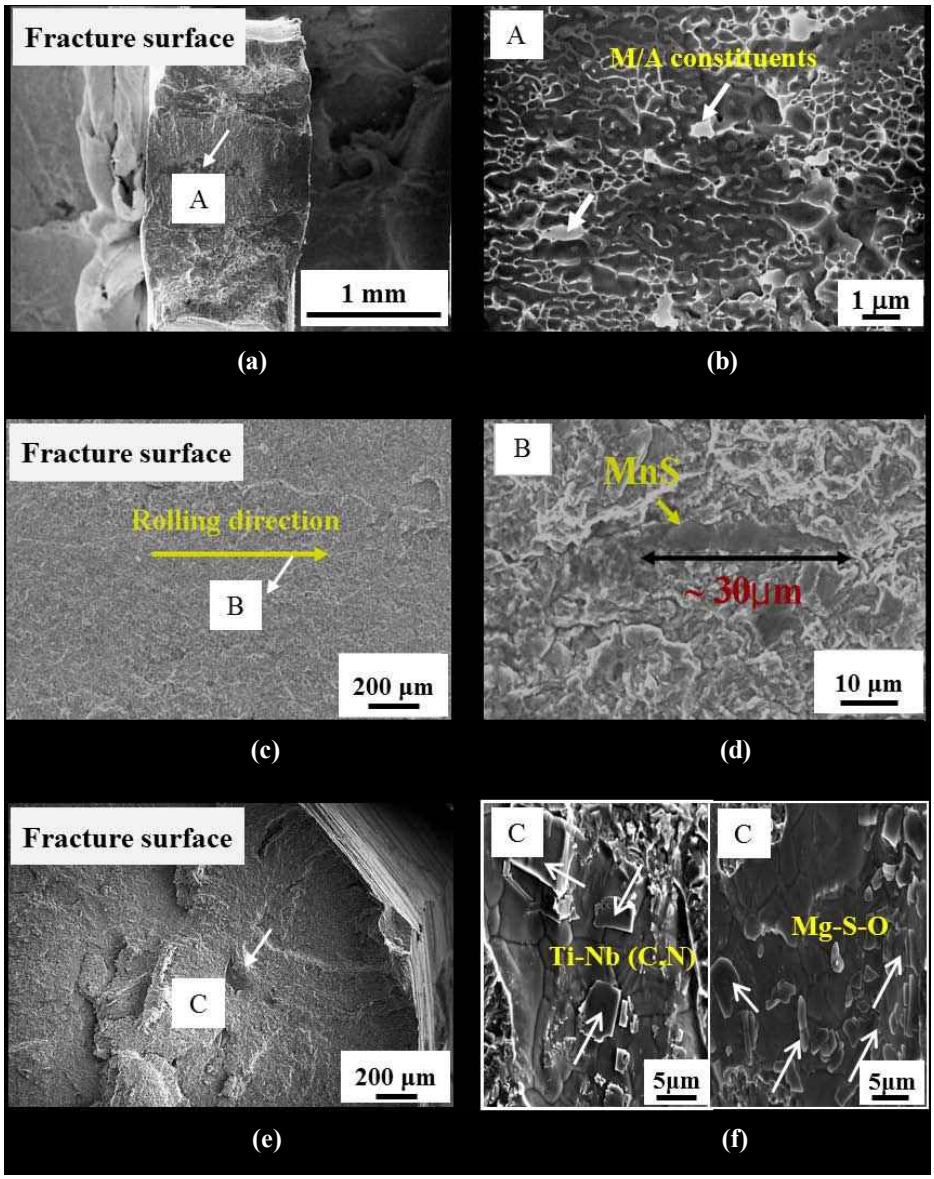

Fig. 15 HIC nucleation sites of ferritic steels: (a), (c) and (e) macroscopic view of fracture surfaces, and (b), (d) and (f) magnified image in (a), (c) and (e), respectively [8,11,42].

obtained by the different heat treatment condition. Fig. 13 exhibits the permeation curves of 516-G60 steel evaluated by electrochemical charging [40]. It is evident that the minimum diffusion kinetics is obtained when the steel has a fresh martensite structure and the diffusivity increases significantly with higher tempering temperature. Particularly, when the steel is tempered over 500 °C, recovery of the dislocation contained between the lath boundaries occurs and the spheroidal Fe_3C particles acting as reversible traps for hydrogen atoms are formed. Luu *et al*. [41] has also studied about the influence of microstructures ranging from spheroidized ferrite to martensite on hydrogen transport in carbon steel employing both electrochemical permeation and hydrogen microprint technique (HMT) methods. The utilization of HMT makes it possible to display the hydrogen diffusion path in the microstructure by the reduction of silver ions from a monolayer of AgBr emulsion by the following reaction:

$$H^0 + Ag^+ \rightarrow H^+ + Ag^0 \quad (13)$$

They have indicated that the main diffusion path for hydrogen atoms is ferrite/Fe_3C and martensite lath interfaces.. In relation to the main diffusion path for hy-

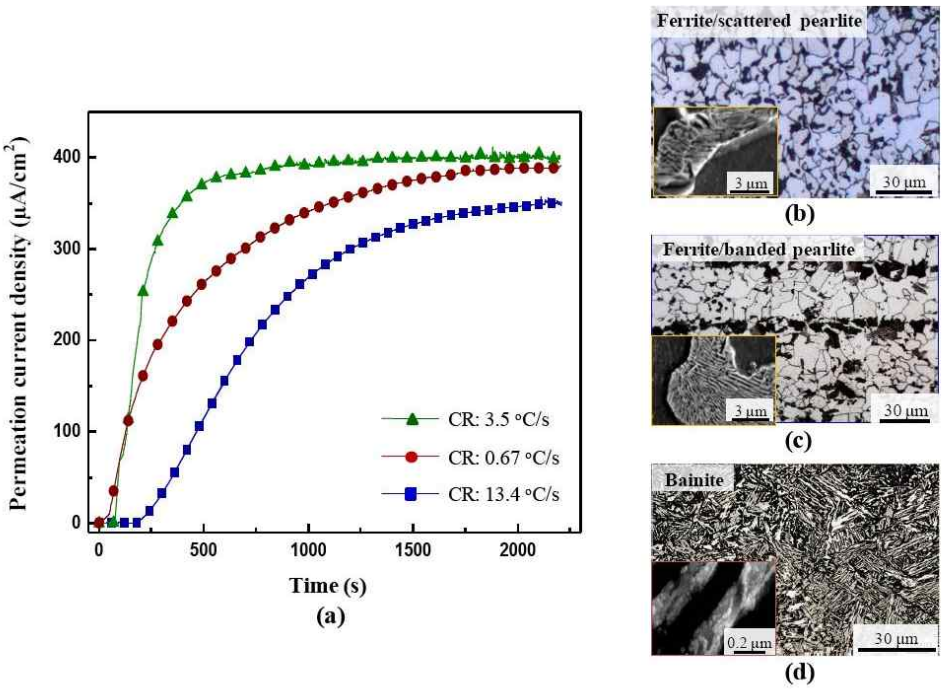

Fig. 16 (a) Hydrogen permeation curves of the tested steels obtained by controlling the cooling rates (CR) with 0.67 °C/s, 3.5 °C/s and 13.4 °C/s, (b), (c) and (d) Microstructures of the steels normalized with CR of 3.5 °C/s, 0.67 °C/s and 13.4 °C/s, respectively [42,92,104].

drogen atom, Wang *et al.* [88] have clearly presented that the diffusion paths identified from the reduced silver grains are the grain boundaries of equiaxed ferrite, and ferrite/carbide interfaces of pearlite and bainite, as well as the boundaries of the grain boundary ferrite and interfaces in the acicular ferrite. Fig. 14 shows the hydrogen diffusion paths in several microstructures of thermo-mechanically controlled process (TMCP) steel [88]. In 2000s, Koh *et al.* [46] and Park *et al.* [8] has indicated that the high-strength low alloy steel with fine grained-acicular ferrite structure manufactured by TMCP exhibits superior resistance to HAC. In fact, the acicular ferrite structure produced by TMCP is not as irregular needle type as the one formed in the weldment, but has a deformed polygonal type with fine grain size. Especially, Park *et al.* [8] have proposed an alternative explanation and they have indicated that hydrogen trapping efficiency is increased in the order of degenerated pearlite, bainitic ferrite and acicular ferrite, with acicular ferrite being the most efficient. This suggests that the acicular ferrite produced by TMCP shows higher resistance to HAC even though more hydrogen atoms are trapped in the microstructure. In other words, the acicular ferrite has high threshold hydrogen concentration for inducing HIC. They concluded that, as the microstructure of high-strength low alloy steel changes from acicular ferrite to bainite, the HIC susceptibility increases, which is attributed to both high threshold hydrogen concentration for inducing HIC and high toughness of the acicular ferrite, impeding the crack propagation. Therefore, to decrease the HIC susceptibility of the steel, the formation of acicular ferrite in the microstructure and prevention of local agglomeration of hard martensite/austenite (M/A) constituents are desirable. Some investigators [8,11,42] have also presented the experimental evidence for the HIC/SSC nucleation sites. Fig. 15 indicates that most cracks nucleated at hard M/A constituents, elongated MnS, (Ti,Nb)(C,N) precipitates or some oxide inclusions [8,11,42]. In 2010s, Kim *et al.* [42,92,104] have also investigated the effect of microstructure on hydrogen permeation and HAC susceptibility of pressure vessel steel (ASTM A516-70). In their study, various microstructures ranging from ferrite/pearlite to bainite were obtained by different cooling process; air cooling (cooling rate: 0.67 °C/s), oil cooling (cooling rate: 3.5 °C/s) and water quenching (cooling rate: 13.4 °C/s) in normalizing heat treatment. The electrochemical permeation behavior of the steels is found in Fig. 16 [92,104]. Based on the permeation transients, several diffusion parameters are obtained by Fick's equation, and the parameters are listed in Table 2 [92,104]. They have found that as the microstructure changes from bainite to ferrite/pearlite and also after tempering conducted at 650 °C, D_{app}

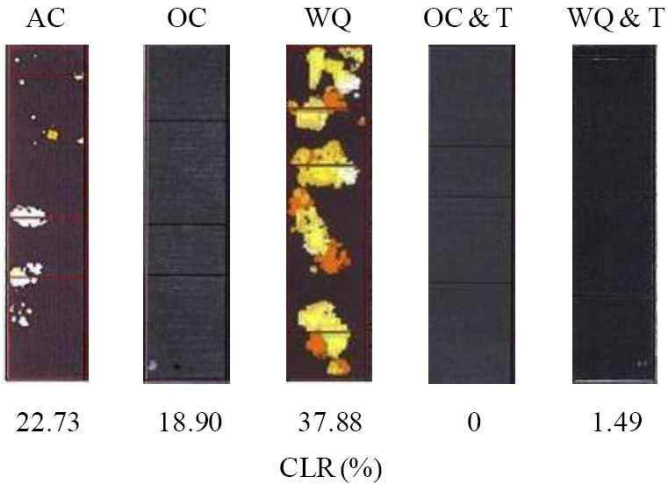

Fig. 17 HIC test results of the steels (AC: Air cooled, OC: Oil cooled, WQ : Water quenched, T : Tempered, CLR : Crack length ratio (%)) [42,92,104].

exhibits a continuous increase while C_{app} shows a gradual decrease, suggesting that HAC resistance could be increased. The crack length ratio (CLR) measured by ultrasonic detector is used as an index of HIC resistance, and the CLR values of the tested steels are found in Fig. 17 [42,92,104]. From the results, it is found that the HIC sensitivity meets well with the value of C_{app} obtained by the electrochemical permeation technique.

6. Summary

For better understanding on hydrogen assisted cracking and hydrogen delayed fracture occurring on a variety of steels, verification of exact physical nature of hydrogen diffusion and trapping in the steels is required. First of all, hydrogen adsorption, diffusion and trapping mechanism of steels are briefly introduced. Then, a number of experimental methods including the electrochemical permeation technique are reviewed. Particularly, a modified permeation technique accommodating the externally applied tensile stress, and its application to high-strength steels are explored. Indeed, successful utilization of the modified permeation technique equipped with a constant load testing device, and "stepwise sequence method" has opened a new frontier, which makes it possible to evaluate the effect of applied tensile stress in both elastic and plastic regime on hydrogen diffusion behavior of the steels. In the last section, a brief introduction to the study on clarifying the relationship among the microstructure, hydrogen permeation, and HAC susceptibility is presented. It is hoped that this study will result in significant academic and practical contributions in the field of hydrogen related problems of a variety of high-strength steels.

Table 2 Hydrogen permeation parameters for the pressure vessel steels (AC: Air cooled specimen, OC: Oil cooled specimen, WQ: Water quenched specimen, T: Tempered specimen after normalizing heat treatment) [92]

			D_{app} ($\times 10^{-9}$ m^2/s)	$J_{ss}L$ ($\times 10^{-8}$ mol/m·s)	C_{app} ($\times 10$ mol/m^3)
Cooling rates (CR: °C/s)	0.67	After norm	0.4~0.5	3.83	8~9.6
	3.5	After norm	0.6~0.7	3.94	5.6~6.6
		After norm & temp	3.5~4.0	4.22	1.0~1.2
	13.4	After norm	0.15~0.25	3.45	14~23
		After norm & temp	2.5~3.0	4.25	1.4~1.7

Acknowledgements

This research was supported by Basic Science Research Program through the National Research Foundation of Korea (NRF) funded by the Ministry of Education (grant number: 2016R1D1A3B03930523).

References

1. F. E. Fujita, *The iron-hydrogen phase diagram*, in: R. A. Oriani, J. P. Hirth, M. Smialowski, *Hydrogen degradation of ferrous alloys*, p. 1, Noyes publications, New Jersey (1985).
2. K. Kiuchi and R. B. Mclellan, *Acta Metall.*, **31**, 961 (1983).
3. R. A. Oriani, *Trans. Fusion. Tech.*, **26**, 235 (1994).
4. Y. Huang, A. Nakajima, A. Nishikata, and T. Tsuru, *ISIJ Int.*, **43**, 548 (2003).
5. S. J. Kim, H. G. Jung, and K. Y. Kim, *Electrochim. Acta*, **78**, 139 (2012).
6. Z. A. Iofa and F. L. Kam, *Zashchita Metallov.*, **10**, 17 (1974).
7. A. Kawashima, K. Hashimoto, and S. Shimodaira, *Corrosion,* **32**, 321 (1976).
8. G. T. Park, S. U. Koh, H. G. Jung, and K. Y. Kim, *Corros. Sci.*, **50**, 1865 (2008).
9. H. Y. Liou, R. I. Shieh, F. I. Wei, and S. C. Wang, *Corrosion*, **49**, 389 (1993).
10. C. Mendibide and T. Sourmail, *Corros. Sci.*, **51**, 2878 (2009).
11. W. K. Kim. H. G. Jung, G. T. Park, S. U. Koh, and K. Y. Kim, *Scripta Mater.*, **62**, 195 (2010).
12. E. Akiyama, K. Matsukado, S. Li, and K. Tsuzaki, *App. Surf. Sci.*, **257**, 8275 (2011).
13. K. H. So, J. S. Kim, Y. S. Chun, K. T. Park, Y. K. Lee, and C. S. Lee, *ISIJ Int.*, **49**, 1952 (2009).
14. S. Li, Z. Zhang, E. Akiyama, K. Tsuzaki, and B. Zhang, *Corros. Sci.*, **52**, 1660 (2010).
15. T. Tsuru, Y. Huang, M. R. Ali, and A. Nishikata, *Corros. Sci.*, **47**, 2431 (2005).
16. T. Omura, T. Kudo, and S. Fujimoto, *Mater. Trans.*, **47**, 2956 (2006).
17. A. R. Troiano, *Trans ASM.*, **52**, 54 (1960).
18. S. P. Lynch, *Proc. NACE International Conf.*, p. 55, NACE, Nashville, USA (2007).
19. C. Zapffe and C. Sims, *Trans. AIME*, **145**, 225 (1941).
20. S. Gahr, M. L. Grossbek, and H. K. Birnbaum, *Acta Metall.*, **25**, 125 (1977).
21. N. J. Petch and P. Stable, *Nature*, **169**, 842 (1952).
22. W. Y. Choo and J. Y. Lee, *Metall. Trans.*, **13A**, 683 (1982).
23. ISO Standard 3690, Determination of hydrogen in deposited weld metal arising from the use of covered electrodes for welding mild and low alloy steels (1977).
24. JIS Standard Z3113, Method for measurement of hydrogen evolved from deposited metal (1975).
25. M. A. V. Devanathan and Z. Stachurski, *Proc. Royal. Soc.*, **A270**, 90 (1962).
26. ISO Standard 17081, Method of measurement of hydrogen permeation and determination of hydrogen uptake and transport in metals by an electrochemical technique (2004).
27. M. Kurkela and R. M. Latanision, *Scripta Mater.* **13**, 927 (1979).
28. R. Otsuka and M. Isaji, *Scripta Metall.*, **15**, 1153 (1981).
29. M. Hashimoto and R. M. Latanision, *Theoretical study of hydrogen transport during plastic deformation in ironMetall. Trans.*, **19**, 2789 (1988).
30. A. M. Brass and J. Chêne, *Corros. Sci.*, **48**, 481 (2006).
31. G. T. Park, H. G. Jung, S. U. Koh, and K. Y. Kim, *19th International Offshore and Polar Engineering (ISOPE) Conf.*, p. 268, ISOPE, Osaka, Japan (2009).
32. M. Kurkela, G. S. Frankel, and R. M. Latanision, *Scripta Mater.*, **16**, 455 (1982).
33. W. Beck, J. O'. M. Bockris, J. McBreen, and L. Nanis L, *Proc. Royal. Soc.*, **290**, 220 (1966).
34. K. T. Kim and S. I. Pyun, *Scripta Metall.*, **22**, 1719 (1988).
35. S. J. Kim and K. Y. Kim, *Scripta Mater.*, **66**, 1069 (2012).
36. S. X. Xie and J. P. Hirth, *Corrosion*, **38**, 486 (1982).
37. D. L. Johnson, G. Krauss, J. K. Wu, and K. P. Tang, *Metall. Trans.*, **18A**, 717 (1987).
38. D. L. Johnson and J. –K. Wu, *J. Mater. Ene. Sys.*, **8**, 402 (1987).
39. H. W. Jeng, L. H. Chiu, D. L. Johnson, and J. K. Wu, *Metall. Trans.*, **21A**, 3257 (1990).
40. M. I. Luppo and J. O–Garcia, *Corros. Sci.*, **32**, 1125 (1991).
41. W. C. Luu and J. K. Wu, *Corros. Sci.*, **38**, 239 (1996).
42. S. J. Kim, H. G. Jung, and K. Y. Kim, *NACE International Conf.*, NACE-11292, NACE, Salt Lake City, Utah, USA (2012).
43. S. J. Kim and K. Y. Kim, *J. Weld. Join.*, **32**, 13 (2014).
44. D. A. Jones, *Principles and prevention of corrosion*, 2nd ed., p. 86, Prentice Hall, NJ (1996).
45. W. K. Kim, S. U. Koh, B. Y. Yang, and K. Y. Kim, *Corros. Sci.*, **50**, 3336 (2008).
46. S. U. Koh, J. S. Kim, B. Y. Yang, and K. Y. Kim, *Corrosion*, **60**, 244 (2004).
47. J. O'. M. Bockris, J. McBreen, and L. Nanis, *J. Electrochem. Soc.*, **112**, 1025 (1965).
48. P. W. Bolmer, *Corrosion*, **21**, 69 (1965).
49. J. P. Hirth, *Hydrogen-defect interactions*, in: R. A. Oriani, J. P. Hirth, M. Smialowski, *Hydrogen degradation of ferrous alloys*, p. 131, Noyes publications, New Jersey (1985).
50. J. P. Hirth, *Metall. Trans.*, **11A**, 861 (1980).
51. A. J. Kumnick, H. H. Johnson, *Acta Metall.*, **28**, 33 (1980).
52. I. Maroef, D. L. Olson, M. Eberhart, and G. R. Edwards, *Mater. Rev.*, **47**, 191 (2002).
53. M. I. Luppo and J. Ovejero–Garcia, *Corros. Sci.*, **32**, 1125 (1991).
54. V. Olden, C. Thaulow, and R. Johnsen, *Mater. Des.*, **29**, 1934 (2008).
55. J. L. Lee and J. Y. Lee, *Metall. Trans.*, **17A**, 2183 (1986).
56. S. Serna S, H. Martínez, S. Y. López, J. G. González–

Rodríguez, and J. L. Albarrán, *Int. J. Hydro. Ene.*, **30**, 1333 (2005).
57. G. M. Pressouyre and I. M. Bernstein, *Metall. Trans.*, **12A**, 835 (1981).
58. G. W. Hong and J. Y. Lee, *J. Mater. Sci.*, **18**, 271 (1983).
59. S. K. He, G. S. Wang, and S. N. Wang, *Acta Metall. Sinica.*, **9**, 619 (1996).
60. T. Asaoka, C. Dagbert, M. Aucouturier, and J. Galland, *Scripta Mater.*, **11**, 467 (1977).
61. L. Tau L, S. L. I. Chan SLI, and C. S. Shin, *Corros. Sci.*, **38**, 2049 (1996).
62. D. L. Johnson, G. Krauss, J. K. Wu, and K. P. Tang, *Metall. Trans.*, **18A**, 717 (1987).
63. Y. D. Park, I. S. Maroef, A. Landau, and D. L. Olson, *Weld. Res.*, **81**, 27 (2002).
64. T. Bollinghaus, H. Hoffmeister, and C. Middel, *Weld. in the World*, **37**, 16 (1996).
65. J. H. Ryu, Y. S. Chun, C. S. Lee, H. K. D. H. Bhadeshia, and D. W. Suh, *Acta Mater.*, **60**, 4085 (2012).
66. R. Gibala and J. Kumnick, *Hydrogen trapping in iron and steels*, in: R. Gibala, R. F. Hehemann, *Hydrogen embrittlement and stress corrosion cracking*, p. 61, ASM Int., OH, (1984).
67. H. H. Podgurski and R. A. Oriani, *Metall. Trans.*, **3**, 2055 (1972).
68. P. Lacombe, M. Aucouturier, J. P. Laurent, and G. L. Passet, *Proc. NACE International Conf.*, p. 423, NACE, Houston, TX (1977).
69. E. Chrnet and R. W. Coughlin, *J. Catalysis*, **27**, 246 (1972).
70. J. L. Lee and J. Y. Lee, *Metal. Sci.*, **17**, 426 (1983).
71. H. G. Lee and J. Y. Lee, *Acta Metall.*, **32**, 131 (1984).
72. D. J. Kotecki and R. A. La Fave, *Weld. J.*, **64**, 31 (1985).
73. I. L. Stern, I. Kalinsky, and E. A. Fenton, *Weld. J.*, **28**, 405 (1949).
74. F. Coe, *Metal Const.*, **18**, 20 (1986).
75. G. K. Padhy and Y. Komizo, *Trans. JWRI.*, **42**, 39 (2013).
76. M. Koyama, H. Springer, S. V. Merzlikin, K. Tsuzaki, E. Akiyama, and D. Raabe, *Int. J. Hyd. Ene.*, **39**, 4634 (2014).
77. H. E. Kissinger, *Anal. Chem.*, **29**, 1702 (1957).
78. A. Cornish-Bowden, *Fundamentals of enzyme kinetics*, p. 4, Wiley-VCH VerlagGmbH & Co., Berlin, Germany (2012).
79. E. J. Song, D. W. Suh, and H. K. D. H. Bhadeshia, *Comp. Mater. Sci.*, **79**, 36 (2013).
80. D. Pérez Escobar, T. Depover, L. Duprez, K. Verbeken, and M. Verhaege, *Acta Mater.*, **60**, 2593 (2012).
81. H. M. Ha, J. H. Ai, and J. R. Scully, *Corrosion*, **70**, 166 (2014).
82. Y. S. Chun, J. S. Kim, K. T. Park, Y. K. Lee, and C. S. Lee, *Mater. Sci. Eng.*, **533A**, 87 (2012).
83. G. Lovicu, M, Barloscio, M. Bottazzi, F. D'Aiuto, M. De Sanctis, A. Dimatteo, C. Federici, S. Maggi, C. Santus, and R. Valentini, *2nd Super–High Strength Steels Conf.*, Verona, Italy (2010).
84. E. W. Johnson and M. L. Hill, *Trans. AIME.*, **218**, 1104 (1960).
85. C. Wert and C. Zener, *Phy. Rev.*, **76**, 1169 (1949).
86. J. Kittel, F. Ropital, and J. Pellier, *NACE International Conf.*, NACE-08409, NACE, Houston, TX, USA (2008).
87. T. Zakroczymski, *Electrochim. Acta*, **51**, 2261 (2006).
88. S. H. Wang, W. C. Luu, K. F. Ho, and J. K. Wu, *Mater. Chem. Phy.*, **77**, 447 (2002).
89. S. Frappart, X. Feaugas, J. Creus, F. Thebault, L. Delattre, and H. Marchebois, *Mater. Sci. Eng.*, **A534**, 384 (2012).
90. W. C. Luu and J. K. Wu, *Corros. Sci.*, **38**, 239 (1996).
91. A. M. Brass and J. Chene, *Mater. Sci. Eng.*, **A242**, 210 (1998).
92. S. J. Kim, H. S. Suh, and K. Y. Kim, *Met. Mater. Int.*, **21**, 666 (2015).
93. A. Turnbull, M. W. Carroll, and D. H. Ferriss, *Acta Metall.*, **37**, 2039 (1989).
94. S. J. Kim, D. W. Yun, H. G. Jung, and K. Y. Kim, *J. Electrochem. Soc.*, **161**, E173 (2014).
95. A. J. Kumnick and H. H. Johnson, *Metall. Trans.*, **5**, 1199 (1974).
96. P. Manolatos, M. Jerome, and J. Galland, *Electrochim. Acta*, **40**, 867 (1995).
97. J. B. Leblond JB and D. Dubois, *Acta Metall.*, **31**, 1459 (1983).
98. P. Bastien and P. Azou, *C. R. Acad. Sci. Paris.*, **232**, 1845 (1951).
99. G. S. Frankel and R. M. Latanision, *Metall. Trans.*, **17A**, 869 (1986).
100. T. Zakroczymski, *Corrosion*, **41**, 485 (1985).
101. C. B. Zheng, H. K. Jiang, and Y. L. Huang, *Corros. Eng. Sci. Tech.*, **46**, 365 (2011).
102. H. E. Townsend, *Corrosion*, **26**, 361 (1970).
103. S. J. Kim, D. W. Yun, D. W. Suh, and K. Y. Kim, *Electrochem.Comm.*, **24**, 112 (2012).
104. S. J. Kim, H. G. Jung, and K. Y. Kim, *Proc. NACE International Conf.*, NACE-2012-1204, NACE, San Antonio, TX, USA (2011).